Kinetik: Game Technology, Information System, Computer Network, Computing, Electronics, and Control
Journal homepage: http://kinetik.umm.ac.id
ISSN: 2503-2267
Vol. 7, No. 3, August, Pp. 251-258

Segmentation of facial bones from skull point clouds based on smoothed deviation angle

Masy Ari Ulinuha[1], Eko Mulyanto Yuniarno*[2], I Ketut Eddy Purnama[3], Mochamad Hariadi[4]
Department of Electrical Engineering, Faculty of Intelligent Electrical and Informatics Technology, Institut Teknologi Sepuluh Nopember, Surabaya, Indonesia[1,2,3]
Department of Information Technology, Faculty of Science and Technology, Universitas Islam Negeri Walisongo, Semarang, Indonesia[1]
Department of Computer Engineering, Faculty of Intelligent Electrical and Informatics Technology, Institut Teknologi Sepuluh Nopember, Surabaya, Indonesia[2,3,4]

Article Info
Keywords:
Segmentation, Facial Bone, Skull Point Cloud, Smoothed Deviation Angle, Thresholding

Article history:
Received: June 05, 2022
Accepted: July 12, 2022
Published: August 31, 2022

Cite:
M. A. Ulinuha, E. M. Yuniarno, I. K. E. Purnama, and M. Hariadi, "Segmentation of Facial Bones from Skull Point Clouds Based on Smoothed Deviation Angle", *KINETIK*, vol. 7, no. 3, Aug. 2022.
https://doi.org/10.22219/kinetik.v7i3.1464

*Corresponding author.
Eko Mulyanto Yuniarno
E-mail address:
ekomulyanto@ee.its.ac.id

Abstract
The human skull was the subject of study in various fields. Segmentation could be a basic tool for better understanding the skull. One of the most challenging tasks was facial bone segmentation. Our previous study had succeeded in segmenting facial bones from skull point clouds, however the quality of the results needed to be improved. In this paper, we proposed a new method to improve the results of facial bone segmentation from skull point clouds. The method consists of three stages: deviation angle extraction, smoothing, and thresholding. Each point in the point cloud was assigned a value based on the deviation angle. These values then went through a smoothing process to clarify the differences between the facial bone region and other regions. Next, thresholding was performed to divide the skull into two regions, namely facial bone and non-facial bone. The proposed method had succeeded in improving the quality of the segmentation results by achieving precision=0.931, recall=0.9854, and F=0.9573.

1. Introduction

The human skull is the subject of study in various fields, including medicine, forensics, anthropology, and biometrics. The skull is the main data in craniofacial reconstruction [1], detection of abnormalities [2], disease detection [3], forensic facial reconstruction [4], and cephalometrics [5].

Skull data can be stored in the form of a point cloud [6], [7]. In this case, the skull is represented by points in three-dimensional coordinates. Point clouds have the advantage of being able to accurately represent 3-dimensional objects [8]. With this advantage, point clouds have been widely used to represent indoor [9] and outdoor scene [10], [11], [12]. Point clouds can represent tables, chairs, cars, motorcycles [13], [14], trees [15], buildings [16], and roads [17].

To explore various information in the point cloud, segmentation becomes the basic tool to better understand the represented object [18]. In general, there are two methods of point cloud segmentation, segmentation based on geometric characteristics, and segmentation based on semantic labeling [19]. Geometry-based segmentation attempts to group point cloud based on their geometric shapes, such as spheres, cones, and tubes. Meanwhile, segmentation based on semantic labeling intends to give meanings to the points in the point cloud. This study is conducted in order to provide these semantic labels. In this case, the semantic labeling is performed on the point cloud of the skull.

A skull can be divided into two regions, the facial bone and the non-facial bone. However, segmentation of the facial bones is still a very challenging task. The facial bone consists of 14 bones that make up the structure of the face. These bones are the two maxillae, the two palatine bones, the two zygomatic bones, the two inferior nasal conchae, the two lacrimal bones, the two nasal bones, the vomer, and the mandible [20]. Based on this knowledge, in previous study we have segmented the facial bone from the point cloud of the skull [21]. This study has succeeded in segmenting facial bone based on the deviation angle. However, the quality of the results can still be improved.

In this paper, we propose a new method to improve the facial bone segmentation results based on the deviation angle. The method consists of three stages, the first is deviation angle extraction, the second is smoothing, and the third is thresholding. Figure 1 shows the facial bone segmentation method. In this method, the values of the deviation angle undergo a smoothing process using a Gaussian filter. Furthermore, a thresholding technique is used to segment the facial bone. The contribution of this study is to improve the results of facial bone segmentation from the point cloud of the skull based on the deviation angle. We improve the quality of the results by increasing the true positive area, and reducing the false positive and false negative areas. Thus, its precision, recall, and F will increase.

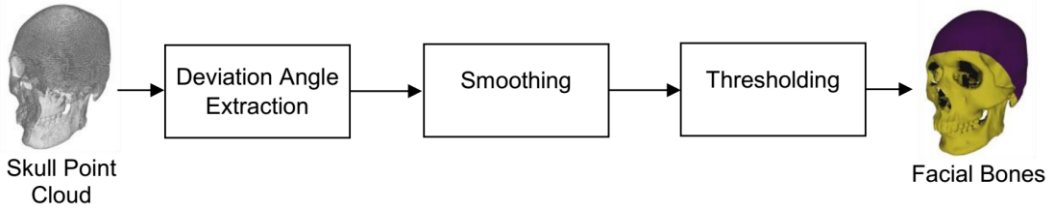

Figure 1. Facial Bone Segmentation Method

2. Deviation Angle Extraction

The skull point cloud in this study only contains its position in three-dimensional coordinates. There is no other information about these points. We intend to assign a value to each of these points based on the characteristics of the skull surface. The value at a point represents the deviation angle at that point. Deviation angle is the angle formed by the normal vector with a specific reference vector.

Based on our observations, there are differences in surface texture between the facial bone region and other regions of the skull. Facial bone tends to be rougher, while the non-facial bone tends to be smoother. We take advantage of this difference to provide a value at each point in the point cloud. Texture variations cause the normal vector direction on the facial bone to be more varied. We want to measure the direction of these normal vectors so that we can get large values for points on the facial bone, and small values for points on non-facial bone. For this purpose, we create a reference vector at each point, then we measure the angle formed by the normal vector and the reference vector. We call this angle the deviation angle [21].

The extraction of the deviation angle consists of four stages: estimation of the normal vector, determining the reference vector, evaluating the direction of the normal vector, and calculating the value of the deviation angle.

2.1 Normal Vector Estimation

The normal vector is an important property in a point cloud. The normal vector indicates the surface orientation and describes the surface structure of the point cloud [22]. Therefore, a reliable method is needed for normal vector estimation [23]. In this section, we will estimate the normal vector at each point in the skull point cloud. In this study, we use planePCA to estimate normal vectors [24].

A skull point cloud can be expressed in matrix form by Equation 1.

$$\mathbf{P} = [\mathbf{p}_1, \mathbf{p}_2, \dots, \mathbf{p}_m]^T \tag{1}$$

where $\mathbf{p}_i = [p_{ix}, p_{iy}, p_{iz}]^T$ is a point in the point cloud and is represented by its position in three-dimensional coordinates, and m is the number of points in the point cloud.

For each $\mathbf{p}_i \in \mathbf{P}$, we will estimate a normal vector $\mathbf{n}_i = [n_{ix}, n_{iy}, n_{iz}]^T$, based on a number of k neighboring points. Equation 2 represents the neighbors of $\mathbf{p}_i$.

$$\mathbf{Q}_i = [\mathbf{q}_{i1}, \mathbf{q}_{i2}, \dots, \mathbf{q}_{ik}]^T \tag{2}$$

where $\mathbf{q}_{ij} \in \mathbf{P}$ and $\mathbf{q}_{ij} \neq \mathbf{p}_i$. $\mathbf{Q}_i$ is obtained by collecting all the points around $\mathbf{p}_i$ with a distance less than or equal to *r* from $\mathbf{p}_i$. The distance between $\mathbf{p}_i$ and $\mathbf{p}_j$ in the point cloud can be calculated by Equation 3.

$$d(\mathbf{p}_i, \mathbf{p}_j) = \|\mathbf{p}_i - \mathbf{p}_j\|_2 \tag{3}$$

$\mathbf{p}_j$ is a neighbor of $\mathbf{p}_i$ if it satisfies Equation 4.

$$\mathbf{p}_j \in \mathbf{Q}_i \text{ if } d(\mathbf{p}_i, \mathbf{p}_j) \leq r \tag{4}$$

If we add $\mathbf{p}_i$ to the neighbors in Equation 2, we get the augmented neighbor matrix as in Equation 5.

$$\mathbf{Q}_i^+ = [\mathbf{p}_i, \mathbf{q}_{i1}, \mathbf{q}_{i2}, \dots, \mathbf{q}_{ik}]^T \tag{5}$$

In planePCA, normal vector estimation is performed by minimizing the variance of $\mathbf{Q}_i^+$, which is represented by Equation 6.

$$\min_{\mathbf{n}_i} \|[\mathbf{Q}_i^+ - \bar{\mathbf{Q}}_i^+]\mathbf{n}_i\|_2 \quad (6)$$

where $\bar{\mathbf{Q}}_i^+$ is a matrix containing the mean of $\bar{\mathbf{q}}_\mathbf{i}^+ = \frac{1}{k+1}\left(\mathbf{p}_\mathrm{i} + \sum_{j=1}^{k} \mathbf{q}_{ij}\right)$ in each row.

The solution to Equation 6 is the singular vector of $[\mathbf{Q}_i^+ - \bar{\mathbf{Q}}_i^+]$ which corresponds to the smallest singular value. This solution is the normal vector $\mathbf{n}_i$ that we are looking for. Furthermore, the normal vector is expressed in unit vector $\hat{\mathbf{n}}_i = \mathbf{n}_i / \|\mathbf{n}_i\|$. The normal vectors at all points in the point cloud are then expressed in Equation 7.

$$\mathbf{N} = [\hat{\mathbf{n}}_1, \hat{\mathbf{n}}_2, \ldots, \hat{\mathbf{n}}_m]^T \quad (7)$$

2.2 Determining the Reference Vector

The shape of the human skull can be assumed to be a sphere with variations in several locations. In a sphere, there is a center point that is right in the middle of the sphere. If we draw a line from the center to a point on its surface, we will find that this line coincides with the normal vector at that point. With this assumption, we define the geometric center as the centroid of the skull. We can determine the centroid point by calculating the average position of all points in the point cloud. The centroid of $\mathbf{P}$ is determined using Equation 8.

$$\bar{\mathbf{P}} = \frac{1}{m}\sum_{i=1}^{m} \mathbf{p}_i \quad (8)$$

From the centroid, we draw lines to the points on the surface of the skull. We take these lines as reference vectors. These references will be used to evaluate the direction of the normal vectors and to calculate the deviation angles. A reference vector is denoted by $\mathbf{a}_i$. For more details, the reference vectors can be seen in Figure 2.

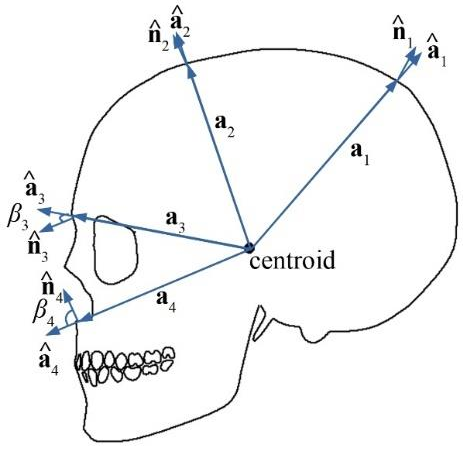

Figure 2. A Skull with Normal Vectors $\hat{\mathbf{n}}_i$ Reference Vectors $\mathbf{a}_i$, and Deviation Angles β_i

2.3 Evaluating the Direction of The Normal Vector

The normal vectors that has been obtained in Equation 7 need to be confirmed that its direction is correct. Assuming that the skull is similar to a sphere, then the direction of the normal vectors on the surface must leave the centroid. To ensure that the direction is correct, we evaluate it based on the reference vector $\mathbf{a}_i$. For each $\mathbf{p}_i$, a reference vector $\mathbf{a}_i$ is created (see Figure 2). The direction of the normal vector at $\mathbf{p}_i$ is declared correct if it satisfies Equation 9.

$$\|\hat{\mathbf{n}}_i + \mathbf{a}_i\| > \|\mathbf{a}_i\| \quad (9)$$

If there is a normal vector that does not satisfy Equation 9, then we reverse its direction. Thus the direction of all normal vectors always leaves the centroid.

2.4 Calculating the Value of The Deviation Angle

The deviation angle in this study is the angle formed by the normal vector with the reference vector at a point on the surface. On a sphere, the deviation angles are all 0^0. On a skull, because the shape is not exactly the same as a

sphere, the values of the deviation angle vary. At the top and back of the skull, where the surface tends to be smooth and similar to a spherical surface, it is suspected that the values of the deviation angle tend to be small. At the front of the skull, there are variations in the shape of the surface. Under these conditions, it is suspected that there are many large deviation angles in this region. The difference in the values of the deviation angle at the front of the skull with other regions, provides very important information in detecting facial bones.

To simplify the calculation, the magnitude of the deviation angle will be represented by the dot product between the normal vector and the reference vector. In order for the dot product to be consistent for all points, the normal and reference vectors are expressed in unit vectors. At $\mathbf{p}_i$, the value of the dot product is given by Equation 10.

$$v_i = \hat{\mathbf{n}}_i \cdot \hat{\mathbf{a}}_i \tag{10}$$

where $\hat{\mathbf{a}}_i = \mathbf{a}_i / \|\mathbf{a}_i\|$ is the reference vector expressed in terms of its unit vector. In three-dimensional Euclidean space, Equation 10 can be solved using Equation 11.

$$v_i = n_{ix}a_{ix} + n_{iy}a_{iy} + n_{iz}a_{iz} \tag{11}$$

The values of the dot product at all points are expressed by Equation 12.

$$\mathbf{V} = [v_1, v_2, v_3, \dots, v_m] \tag{12}$$

3. Facial Bone Segmentation

Facial bone segmentation aims to divide the skull into two regions, namely the facial bone and the non-facial bone. The extraction of the deviation angle has been described in Section 2. In this section, the second and third stages are described.

3.1 Smoothing

The dot product between normal and reference vectors produces a wide variety of values. On the top and back of the skull, the dot product produces large values and only a few small values. While on the front, there are many small values, but there are also many large values. The smoothing process is intended to minimize the variation in these values. By smoothing, it is expected that the values in the facial bone become more uniform with small values. Meanwhile, in the non-facial bone, the values are uniform with large values. This will make it easier to distinguish the facial bone region from the rest of the skull.

The smoothing process is carried out on the dot product values $\mathbf{V}$ using a Gaussian filter. We perform filtering at each point in the point cloud. At each point, we look for its nearest neighbors within radius σ. Point $\mathbf{p}_j$ is declared a neighbor of $\mathbf{p}_i$ if its distance from $\mathbf{p}_i$ is less than σ. In other words, $\mathbf{p}_j$ is a neighbor of $\mathbf{p}_i$ if it satisfies Equation 13.

$$\left\|\mathbf{p}_j - \mathbf{p}_i\right\|_2 < \sigma \tag{13}$$

The value v at point $\mathbf{p}_i$ and all its neighbors are weighted based on their distance from $\mathbf{p}_i$. The weight w_j is obtained from the Gaussian function in Equation 14.

$$w_j = e^{-\frac{\left\|\mathbf{p}_j - \mathbf{p}_i\right\|_2^2}{2\sigma^2}} \tag{14}$$

Then point $\mathbf{p}_i$ is assigned a new value based on the weighted average of neighboring values. The new value v_{gi} is obtained by Equation 15.

$$v_{gi} = \frac{\sum_{j=1}^{n} w_j \cdot v_j}{\sum_{j=1}^{n} w_j} \tag{15}$$

After the smoothing process is carried out at all points, new values are obtained. Equation 16 represents these new values.

$$\mathbf{V}_g = \left[v_{g1}, v_{g2}, v_{g3}, \dots, v_{gm}\right] \tag{16}$$

3.2 Thresholding

Each point in the point cloud has obtained a new value v_{gi} which is the result of the smoothing process. Based on the observations on $\mathbf{V}_g$, it is found that the values in the facial bone region became more uniform. These values are smaller when compared to other regions outside the facial bone. Based on these facts, we applied a thresholding technique to separate the facial bone region from the skull.

Thresholding is performed by determining the threshold value t. A skull point cloud will be grouped into two regions: facial bone and non-facial bone. Points with a value equal to or less than the threshold are categorized as facial bone. While the points whose value is more than the threshold are categorized as non-facial bone. The thresholding process is applied by Equation 17.

$$c(\mathbf{p}_i) = \begin{cases} 0 & \text{if} \quad v_{gi} \leq t \\ 1 & \text{if} \quad v_{gi} > t \end{cases} \tag{17}$$

where $c(\mathbf{p}_i) = 0$ means $\mathbf{p}_i$ is facial bone, and $c(\mathbf{p}_i) = 1$ means $\mathbf{p}_i$ is non-facial bone. Threshold value t is calculated automatically based on an iterative procedure [25]. The initial threshold value is the mean of $\mathbf{V}_g$. To limit the iterations, we specify $\Delta t = 0.0001$.

4. Result and Discussion

The segmentation method is applied to 23 human skulls. Each skull is stored in the form of a point cloud. A skull point cloud is derived from a set of CT images of a head. A set of CT images is processed slice by slice to obtain the outermost contour of the skull. The contours are then arranged in a stack according to the order of the slices. This stack forms a point cloud. Each pixel on the contour becomes a point in the point cloud. The distance between points is adjusted according to the metadata of the CT image file. The complete process of point cloud reconstruction of this CT image can be found in our previous study [6]. The neck is removed from each point cloud. All of these processes produce 23 skull point clouds with the number of points varying from 198,528 to 293,126.

4.1 Segmentation Result

The proposed method has successfully segmented the facial bones from the point cloud of the skull. Each stage in the facial bone segmentation has been successful. The result of each stage can be seen in Figure 3. The point cloud of the skull is shown in Figure 3(a). This is the input data that will be processed to obtain the facial bone.

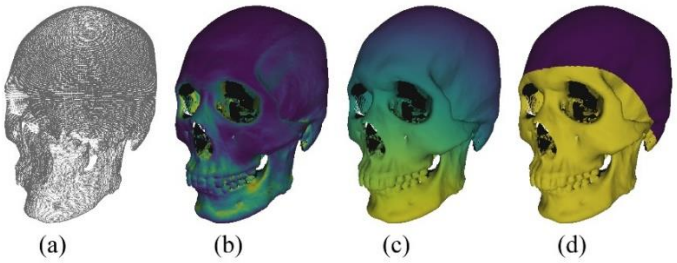

Figure 3. (a) A Skull Point Cloud, (b) Dot Product Values, (c) New Values After Smoothing, (d) Segmentation Result

Figure 3(b) shows the dot product values at all points in the point cloud. In this figure it can be seen that at the top and back of the skull, the values tend to be uniform. In this region, the values of the dot product are large. However, there are still a few points that have small value. While in the facial bone region, the dot product values are more varied. There are many points that have small value. However, there are still many points that have large value.

The result of the smoothing process is shown in Figure 3(c). In this figure, it can be seen that the change in dot product values from one region to another becomes smoother. The dot product values in the facial bone becomes more uniform and the values are smaller compared to other regions. In the non-facial bone region, the dot product values become more uniform with values larger than the facial bone region.

The thresholding process is carried out after the dot product values in the facial bones can be distinguished from the values in other regions. Thresholding result is shown in Figure 3(d). This figure shows that the skull has been successfully divided into two regions, the facial bone and the non-facial bone. This is the output data, and is the final result of facial bone segmentation.

The results of facial bone segmentation are visually shown in Figure 4. The figure shows examples of segmentation results. Overall, the segmentation method is successfully applied to 23 skulls.

Figure 4. Segmentation Results

4.2 Manual Segmentation

Manual segmentation is used as a comparison against the proposed method. Manual segmentation is performed by placing the skull in a lateral position, then cutting it into two parts, the facial bone and the non-facial bone. According to Jinkins [20], the facial bones consist of 14 bones. Manual segmentation should ensure that these 14 bones are categorized as facial bones. This can be obtained by defining the boundaries of the entire facial bones, and grouping the areas within these boundaries as the facial bone region. For this purpose, we determine three landmark points on the skull that can be used to define the facial bone boundaries. The three landmarks are Frontotemporale (ft), Porion (po), and Gonion (go) [26]. These three landmarks are clearly visible when the skull is in a lateral position. Therefore, manual segmentation is performed on the skull in a lateral position.

Manual segmentation is performed by drawing straight lines from Porion to Gonion and from Porion to Frontotemporale as shown in Figure 5. The lines that pass through these three landmarks are the boundaries between the facial bone region and the non-facial bone region. With these boundaries, the fourteen bones that make up the face have been included in the facial bone region.

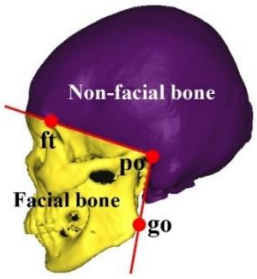

Figure 5. Manual Segmentation

The manual segmentation result is assumed to be the correct segmentation result. Furthermore, the result of segmentation based on the deviation angle is compared with this manual segmentation.

4.3 Evaluation

We measure the success rate of facial bone segmentation by comparing the segmentation results with the manual segmentation results. When the segmentation results are compared, there are four areas of the skull. The four areas are True Positive (TP), True Negative (TN), False Positive (FP), and False Negative (FN). The four areas are shown in Figure 6.

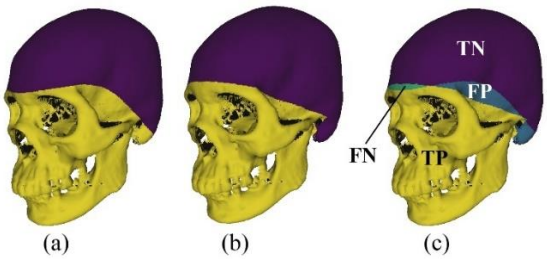

Figure 6. Comparison Between (a) Segmentation Result and (b) Manual Result, (c) TP, TN, FP, and FN Areas

TP is the facial bone region that is correctly detected as facial bone. Meanwhile, TN is the non-facial bone region that is correctly detected as non-facial bone. TP and TN are the correct results of segmentation. FP is a non-facial bone region that is incorrectly detected as facial bone. Whereas FN is the facial bone region that is incorrectly detected as non-facial bone. FP and FN are incorrect results of segmentation. The best results are obtained when there are no FP

and FN areas. But in fact, segmentation errors still occur. To determine the success rate of the proposed method, we measure precision, recall, and F-measure [27].

Precision indicates the facial bone segmentation result which are truly facial bone. While recall is a measure that indicates facial bones that are actually detected. Precision and recall can be calculated using Equation 18 and Equation 19.

$$Precision = \frac{|TP|}{|TP| + |FP|} \tag{18}$$

$$Recall = \frac{|TP|}{|TP| + |FN|} \tag{19}$$

When precision and recall get the maximum value, it can be said that the segmentation has obtained the best result. However, the real result of segmentation is a compromise of precision and recall. This compromise value is expressed in F-measure which is the harmonic mean of precision and recall. F-measure is calculated by Equation 20.

$$F = \frac{2 \cdot Precision \cdot Recall}{Precision + Recall} \tag{20}$$

We calculate precision, recall, and F-measure on 23 segmentation results, the results are shown in Table 1. The values of σ (in centimeters) and t for each skull are also shown in Table 1. The highest precision is achieved by Skull_16 with a value of 0.9624. While the lowest precision is achieved by Skull_23 with a value of 0.8967. For all skulls, the mean precision is 0.931. This indicates that 93.1% of the segmentation results are actually facial bone.

Table 1. Precision, Recall, and F-measure

Point cloud	Precision	Recall	F	σ (cm)	t	Point cloud	Precision	Recall	F	σ (cm)	t
Skull_1	0.9076	0.9889	0.9465	5	0.7613	Skull_14	0.9174	0.9795	0.9474	3	0.773
Skull_2	0.9163	0.9923	0.9528	8	0.7718	Skull_15	0.9392	0.9852	0.9617	4	0.7862
Skull_3	0.9197	0.9719	0.9451	3	0.8092	Skull_16	0.9624	0.987	0.9745	4	0.7615
Skull_4	0.9533	0.9785	0.9658	5	0.7627	Skull_17	0.9605	0.9773	0.9688	4	0.7632
Skull_5	0.96	0.9897	0.9746	6	0.7694	Skull_18	0.9264	0.985	0.9548	3	0.7733
Skull_6	0.9159	0.9842	0.9488	5	0.7793	Skull_19	0.9226	0.9887	0.9545	4	0.7776
Skull_7	0.9112	0.9852	0.9467	4	0.7874	Skull_20	0.9282	0.99	0.9581	5	0.7915
Skull_8	0.9492	0.9807	0.9647	4	0.7714	Skull_21	0.9562	0.9852	0.9705	8	0.7678
Skull_9	0.9139	0.9966	0.9535	6	0.7636	Skull_22	0.9581	0.9873	0.9725	6	0.7818
Skull_10	0.9471	0.9887	0.9674	4	0.7822	Skull_23	0.8967	0.9963	0.9439	4	0.7899
Skull_11	0.9388	0.9896	0.9636	5	0.758	Max	0.9624	0.9966	0.9746		
Skull_12	0.9038	0.9926	0.9461	4	0.7841	Min	0.8967	0.9633	0.9353		
Skull_13	0.9088	0.9633	0.9353	4	0.7554	Mean	0.9310	0.9854	0.9573		

The highest recall is 0.9966 which is achieved by Skull_9. While the lowest recall is 0.9633 which is achieved by Skull_13. The average recall value reached 0.9854. This means that 98.54% of facial bones are actually detected. The mean value of F-measure is 0.9573. Skull_5 achieve the highest F-measure with a value of 0.9746. On the other hand, Skull_13 achieve the lowest F-measure with a value of 0.9353. Based on the F-measure, it can be seen that the best segmentation result is achieved by Skull_5. While the worst segmentation result is achieved by Skull_13.

The precision, recall, and F-measure achieved by the proposed method are higher than our previous study [21]. Comparison of the results of the proposed method with our previous study can be seen in Table 2.

Table 2. Comparison of the Proposed Method with our Previous Study

	Previous study	Proposed method
Precision	0.836	0.931
Recall	0.951	0.9854
F	0.89	0.9573

5. Conclusion

In this paper, we propose a method for segmenting facial bones from skull point clouds. The proposed method is based on the deviation angle. Each point in the point cloud is assigned a value based on the deviation angle. To reduce variations in the value of the deviation angle on the facial bone, a smoothing process is carried out using a Gaussian filter. Then the thresholding technique is used to divide the skull into two regions, namely facial bones and non-facial bones. The threshold value is determined based on an iterative procedure.

The proposed method has succeeded in segmenting facial bones with precision=0.931, recall=0.9854, and F=0.9573. This result is higher than our previous study.

References

[1] K. M. Day *et al.*, "Advanced Three-Dimensional Technologies in Craniofacial Reconstruction," Plastic & Reconstructive Surgery, Vol. 148, No. 1, Pp. 94e-108e, Jul. 2021. https://doi.org/10.1097/PRS.0000000000008212

[2] S. A. H. Tabatabaei *et al.*, "Automatic Detection and Monitoring of Abnormal Skull Shape in Children with Deformational Plagiocephaly using Deep Learning," Scientific Reports, Vol. 11, No. 1, P. 17970, Dec. 2021. https://doi.org/10.1038/s41598-021-96821-7

[3] A. Ari and D. Hanbay, "Deep Learning Based Brain Tumor Classification and Detection System," Turkish Journal of Electrical Engineering & Computer Sciences, Vol. 26, No. 5, Pp. 2275–2286, Sep. 2018. https://doi.org/10.3906/elk-1801-8

[4] A. Kundu, M. Streed, P. J. Galzi, and A. Johnson, "A Detailed Review of Forensic Facial Reconstruction Techniques," Medico-Legal Journal, Vol. 89, No. 2, Pp. 106–116, Jun. 2021. https://doi.org/10.1177/0025817221989591

[5] H. J. Kwon, H. Il Koo, J. Park, and N. I. Cho, "Multistage Probabilistic Approach for the Localization of Cephalometric Landmarks," *IEEE Access*, Vol. 9, Pp. 21306–21314, 2021. https://doi.org/10.1109/ACCESS.2021.3052460

[6] M. A. Ulinuha, E. M. Yuniarno, M. Hariadi, and I. K. Eddy Purnama, "Extraction of Skull and Face Surfaces from CT Images," in *2019 International Conference of Artificial Intelligence and Information Technology (ICAIIT)*, Pp. 37–40, 2019. https://doi.org/10.1109/ICAIIT.2019.8834469

[7] J. Li *et al.*, "Synthetic Skull Bone Defects for Automatic Patient-specific Craniofacial Implant Design," Scientific Data, Vol. 8, No. 1, P. 36, Dec. 2021. https://doi.org/10.1038/s41597-021-00806-0

[8] W. Li, G. Chen, H. Yang, R. Chen, and B. Yu, "Learning Point Clouds in EDA," in *Proceedings of the 2021 International Symposium on Physical Design*, Pp. 55–62, 2021. https://doi.org/10.1145/3439706.3446895

[9] M. Bassier, M. Vergauwen, and F. Poux, "Point Cloud vs. Mesh Features for Building Interior Classification," Remote Sensing, Vol. 12, No. 14, P. 2224, Jul. 2020. https://doi.org/10.3390/rs12142224

[10] A. Novo, N. Fariñas-Álvarez, J. Martínez-Sánchez, H. González-Jorge, and H. Lorenzo, "Automatic Processing of Aerial LiDAR Data to Detect Vegetation Continuity in the Surroundings of Roads," Remote Sensing, Vol. 12, No. 10, P. 1677, May 2020. https://doi.org/10.3390/rs12101677

[11] X. Shen, C. Qin, Y. Du, X. Yu, and R. Zhang, "An Automatic Extraction Algorithm of High Voltage Transmission Lines from Airborne LIDAR Point Cloud Data," Turkish Journal of Electrical Engineering & Computer Sciences, Vol. 26, No. 4, Pp. 2043–2055, Jul. 2018. https://doi.org/10.3906/elk-1801-23

[12] G. Chen *et al.*, "Pedestrian Detection Based on Panoramic Depth Map Transformed from 3D-LiDAR Data," Periodica Polytechnica Electrical Engineering and Computer Science, Vol. 64, No. 3, Pp. 274–285, Apr. 2020. https://doi.org/10.3311/PPee.14960

[13] X. Wang, S. Liu, X. Shen, C. Shen, and J. Jia, "Associatively Segmenting Instances and Semantics in Point Clouds," in *2019 IEEE/CVF Conference on Computer Vision and Pattern Recognition (CVPR)*, Pp. 4091–4100, 2019. https://doi.org/10.1109/CVPR.2019.00422

[14] W. Wang, R. Yu, Q. Huang, and U. Neumann, "SGPN: Similarity Group Proposal Network for 3D Point Cloud Instance Segmentation," in *2018 IEEE/CVF Conference on Computer Vision and Pattern Recognition*, Pp. 2569–2578, 2018. https://doi.org/10.1109/CVPR.2018.00272

[15] A. Fekete and M. Cserep, "Tree Segmentation and Change Detection of Large Urban Areas Based on Airborne LiDAR," Computers & Geosciences, Vol. 156, P. 104900, Nov. 2021. https://doi.org/10.1016/j.cageo.2021.104900

[16] Y. Xu, W. Yao, S. Tuttas, L. Hoegner, and U. Stilla, "Unsupervised Segmentation of Point Clouds From Buildings Using Hierarchical Clustering Based on Gestalt Principles," IEEE Journal of Selected Topics in Applied Earth Observations and Remote Sensing, Vol. 11, No. 11, Pp. 4270–4286, Nov. 2018. https://doi.org/10.1109/JSTARS.2018.2817227

[17] C. Choy, J. Gwak, and S. Savarese, "4D Spatio-Temporal ConvNets: Minkowski Convolutional Neural Networks," in *2019 IEEE/CVF Conference on Computer Vision and Pattern Recognition (CVPR)*, Pp. 3070–3079, 2019. https://doi.org/10.1109/CVPR.2019.00319

[18] L. Liu, J. Yu, L. Tan, W. Su, L. Zhao, and W. Tao, "Semantic Segmentation of 3D Point Cloud Based on Spatial Eight-Quadrant Kernel Convolution," Remote Sensing, Vol. 13, No. 16, P. 3140, Aug. 2021. https://doi.org/10.3390/rs13163140

[19] Y. Xie, J. Tian, and X. X. Zhu, "Linking Points With Labels in 3D: A Review of Point Cloud Semantic Segmentation," IEEE Geoscience and Remote Sensing Magazine, Vol. 8, No. 4, Pp. 38–59, Dec. 2020. https://doi.org/10.1109/MGRS.2019.2937630

[20] J. R. Jinkins, "Atlas of Neuroradiologic Embryology, Anatomy, and Variants", Philadelphia: Lippincott Williams & Wilkins, 2000.

[21] M. A. Ulinuha, E. M. Yuniarno, I. K. E. Purnama, and M. Hariadi, "Facial Bones Segmentation from Skull Point Clouds Based on Deviation Angle," Pollack Periodica, Vol. 16, No. 2, Pp. 98–103, Mar. 2021. https://doi.org/10.1556/606.2020.00234

[22] J. Zhang, J.-J. Cao, H.-R. Zhu, D.-M. Yan, and X.-P. Liu, "Geometry Guided Deep Surface Normal Estimation," Computer-Aided Design, Vol. 142, P. 103119, Jan. 2022. https://doi.org/10.1016/j.cad.2021.103119

[23] Z. Yu, T. Wang, T. Guo, H. Li, and J. Dong, "Robust Point Cloud Normal Estimation via Neighborhood Reconstruction," Advances in Mechanical Engineering, Vol. 11, No. 4, pp. 1–19, Apr. 2019. https://doi.org/10.1177/1687814019836043

[24] K. Jordan and P. Mordohai, "A Quantitative Evaluation of Surface Normal Estimation in Point Clouds," in *2014 IEEE/RSJ International Conference on Intelligent Robots and Systems*, Pp. 4220–4226, 2014. https://doi.org/10.1109/IROS.2014.6943157

[25] R. Gonzalez, W. Richard, and E. Steven, *Digital Image Processing Using MATLAB*, 3rd ed. Knoxville: Gatesmark Publishing, 2020.

[26] M. Y. Iscan and M. Steyn, *The Human Skeleton in Forensic Medicine*. Springfield, Illinois: Charles C Thomas, 2013.

[27] J. Pont-Tuset and F. Marques, "Supervised Evaluation of Image Segmentation and Object Proposal Techniques," IEEE Transactions on Pattern Analysis and Machine Intelligence, Vol. 38, No. 7, Pp. 1465–1478, Jul. 2016. https://doi.org/10.1109/TPAMI.2015.2481406